Estimation of the freeze-out parameters reachable in a fixed-target experiment at the CERN Large Hadron Collider

Viktor Begun,[1,*] Daniel Kikoła,[1,†] Volodymyr Vovchenko,[2,3,‡] and Daniel Wielanek[1,§]
[1]*Faculty of Physics, Warsaw University of Technology, Koszykowa 75, 00-662 Warsaw, Poland*
[2]*Institut für Theoretische Physik, Goethe Universität Frankfurt, D-60438 Frankfurt am Main, Germany*
[3]*Frankfurt Institute for Advanced Studies, Giersch Science Center, D-60438 Frankfurt am Main, Germany*

(Received 19 June 2018; published 12 September 2018)

Estimation of the freeze-out parameters as a function of the rapidity in Pb + Pb collisions at $\sqrt{s_{NN}} = 72$ GeV in the AFTER@LHC project is performed. The conventional hadron resonance gas model is used for analysis of the events generated by the UrQMD model. The results indicate that one may obtain at least a 2.5 times increase in the baryon chemical potential μ_B in the forward rapidity range compared to the midrapidity range. The μ_B values in the rapidity range of $0 < y < 4.5$ for AFTER@LHC are comparable to those covered by the RHIC Beam Energy Scan program. Thus, a rapidity scan in the AFTER@LHC project provides a complementary approach for study of the QCD phase diagram.

DOI: 10.1103/PhysRevC.98.034905

I. INTRODUCTION

Determination of the phase structure of strongly interacting QCD matter is one of the most fundamental open questions in nuclear physics. The QCD phase diagram is usually expressed in terms of the temperature T and the baryon chemical potential μ_B. The experimental data collected in high-energy heavy-ion collision experiments at the Super Proton Synchrotron, at the Relativistic Heavy-Ion Collider (RHIC), and at the Large Hadron Collider (LHC) provide strong evidence that a state of matter with partonic degrees of freedom (quark-gluon plasma; QGP) is created in such collisions [1–10]. Lattice QCD calculations indicate that there is a "smooth" phase transition between the hadronic matter and the QGP at $\mu_B = 0$, the so-called crossover transition [11–13]. Theory calculations suggest that in the range of large μ_B the first-order phase transition takes place [14–18], thus the QCD critical point, which separates these two types of phase transitions, is expected to exist. However, the corresponding theoretical calculations provide little guidance regarding the position of the critical point in the temperature and baryon chemical potential phase diagram; the predictions cover almost the whole $T(\mu_B)$ plane [19]. Therefore, the search for the critical point of the QCD matter is one of the main motivations for ongoing and future experiments on heavy-ion collisions (see, e.g., Refs. [20–25]).

The present experimental method for changing T and μ_B is either to vary the collision energy or to change the types of colliding nuclei. However, these approaches have some significant constraints. The available energies are limited by the accelerator capabilities; see, for example, RHIC Beam Energy Scan (BES) program, phase I and phase II [21]. The existing observables might be sensitive to the critical point only in its closest vicinity (see, e.g., Ref. [26]). Thus, it is possible to miss the critical point in a collision energy scan. Moreover, the number of available statistics decreases significantly with decreasing bombarding energy in the collider mode. This limits high-statistics studies to low transverse momenta and only to the most abundant particle species.

In this paper we recall the alternative approach: varying the rapidity interval at a fixed collision energy [27–31]. The topic recently received renewed interest; the physics discussed include high baryon densities achievable at the LHC and RHIC in the fragmentation region [32,33] and the search for critical-point signatures through the rapidity dependence of proton number cumulants [34]. In a rapidity scan one compares the subsystems corresponding to different rapidity bins and characterizes them via different thermodynamic parameters. In the simplest corresponding physical picture the rapidity axis is populated at freeze-out by fireballs, each characterized by thermal parameters, which depend on the fireball's space-time rapidity $y_{\rm FB}$ [31]. All fireballs contribute to the hadron yield spectrum at a given rapidity y. However, the dominant contributions do come from fireballs with $y_{\rm FB} \simeq y$. Therefore, the $y_{\rm FB}$ dependence of thermal parameters at freeze-out translates into the y dependence of the final-state hadron chemistry. We provide estimates of the T and μ_B values reachable at different rapidities in a fixed target experiment at the LHC—the AFTER@LHC project [35] (see also [36])—by analyzing the hadron yield chemistry in different rapidity bins using the UrQMD model[1] [41,42]. We compare

*viktor.begun@gmail.com
†daniel.kikola@pw.edu.pl
‡vlvovch@gmail.com
§daniel.wielanek@cern.ch

[1]The UrQMD model has been used before to estimate the temperatures and baryochemical potentials reached during fireball evolution

the outcome with the results of the analysis of the total rapidity range and with the energy scan at fixed rapidity $y \sim 0$. The goal of this paper is to answer the question whether a rapidity scan at the AFTER@LHC can be used to change T and μ_B by an amount notably larger than the uncertainty of T and μ_B and comparable to the amount reachable in an energy scan at midrapidity.

For measurement of the particle yields at larger rapidities proposed in this paper, the ALICE detector has to successfully operate in the fixed-target mode. Even though ALICE was designed as a collider experiment, it is well suited for measurements of fixed-target collisions. The ALICE main detector, the time projection chamber (TPC), has an excellent spatial resolution, and it is capable of measuring thousands of particle tracks in a collision. Therefore, it is an appropriate tool for recording fixed-target events, where most of the particles fly together due to large boost.

The STAR experiment provides an example that this is indeed the case. The STAR at the RHIC is similar to the ALICE detector in many aspects: it has a similar geometry, the TPC is the main tracking device, and there is a time-of-flight detector installed outside the TPC to improve particle identification. STAR has performed successful fixed-target measurements of Au-Au collisions using these two detectors for particle track and primary vertex reconstruction and for particle identification [43,44]. STAR uses a thin gold foil placed at the entrance to the STAR TPC to study collisions in the low-energy range ($3 < \sqrt{s_{NN}} < 7$ GeV), where the operation in a collider mode was unfeasible or unpractical due to the low collision rate. The STAR Fixed Target program extends the μ_B range available in the RHIC BES and provides good-quality data that can serve as reference measurements in the search for the phase transition and the critical point. Following its original success, the fixed-target mode is a part of the Beam Energy Scan II program, planned for 2019 and 2020. The positive experience of STAR provides proof that a detector designed for central-rapidity measurement in the collider mode can work very well in the fixed-target mode.

A fixed-target experiment using TeV beams of the LHC exhibits a couple of unique features. Such an experiment will have a wide kinematic coverage. The collision of a 2.76-TeV heavy-ion (for instance, Pb) beam on a fixed target releases a center-of-mass-system (c.m.s.) energy per nucleon pair $\sqrt{s_{NN}} = 72$ GeV. These collisions occur in a frame with an extremely large Lorentz factor, $\gamma \approx 4.3$. Due to the Lorentz boost, the forward instrumentation of existing LHC detectors provides midrapidity coverage in the c.m.s. For example, the LHCb experiment, with a pseudorapidity coverage of $2 < \eta < 5$ in the laboratory frame, would cover the c.m.s. rapidity of $-2.3 \lesssim y \lesssim 0.7$. In the case of ALICE, the central detector (with $|y^{\mathrm{Lab}}| < 0.9$) becomes a "backward" one in the fixed-target mode, with access to the large absolute value of rapidity in the c.m.s. with $-5.2 \lesssim y^{\mathrm{c.m.s.}} \lesssim -3.4$. In general, AFTER@LHC will provide broad kinematic coverage, $-5.2 \lesssim y^{\mathrm{c.m.s.}} \lesssim 0.7$, which is not the case in the collider mode.

Particle identification at a large rapidity is challenging. However, prior studies have proven that the LHCb detector performs exceptionally in identifying various hadrons over a broad rapidity range. More specifically, the LHCb Collaboration has reported measurements of identified yields in p + p collisions at $\sqrt{s} = 0.9$ and 7 TeV in the rapidity range $2 < y \lesssim 4.5$ for proton/antiproton, K^+/K^-, and π^+/π^- yield ratios (see Tables 8–10 in [45], as well as the K^0_S and Λ production measurements in [46]). More recently, the LHCb Collaboration reported also the preliminary results of antiproton production measurement in a p + He collision in a fixed-target mode, at momenta corresponding to large rapidities ($y \simeq 4-5$) (see [47,48]). These experimental results prove that the LHCb is capable of effective hadron identification over a rapidity range of at least $2 \lesssim y \lesssim 5$.

The available luminosity per year is very high, similar to the nominal LHC luminosities and orders of magnitude larger than that at the RHIC in a similar energy range [49]. Such a number of data gives access to rare probes like heavy quarks: quarkonium [50] and open heavy flavor hadrons. In addition, one can easily change the atomic mass of the target, which facilitates system-size dependence study. In general the AFTER@LHC project will have a broad physics program which includes the high-x frontier, spin physics at the LHC (given the installation of the polarized target), and heavy-ion physics (see, e.g., [49,51–54], and other publications and presentations in [35]). These goals can be achieved in a cost-effective way, by collecting data in the fixed-target mode in existing experiments (LHCb and ALICE) in parallel to the collider-mode operation. For the study described in this paper, we assume that AFTER@LHC will deliver sufficiently good particle identification over a broad rapidity range. This expectation is based on the capabilities of the LHCb and the ALICE detectors. Moreover, the LHCb experiment has already proven that it is capable of registration and identification of particles and performance of physics measurements in the fixed-target mode [47].

II. RAPIDITY SCAN VS ENERGY SCAN

We perform the estimates of the temperature T, baryochemical potential μ_B, and volume V of the analyzed systems in two steps. First, we calculate the mean multiplicities of produced particles using the UrQMD model [41,42]. Second, we fit the obtained mean multiplicities in a hadron resonance gas (HRG) model. We use the UrQMD-3.4 model to generate the 10% most central Pb + Pb collisions at the $\sqrt{s_{NN}} = 72$ GeV. The number of events is $N_{\mathrm{ev}} \simeq 2 \times 10^5$. The UrQMD is run in the cascade mode, without hydro, for simplicity. The resulting rapidity distribution for different hadron species with the rapidity steps $\Delta y = 0.5$ shown in Fig. 1.

The Δy step is chosen so that it is small enough to catch the forward rapidity increase in the dN/dy for protons, but not too small so as to have enough statistics for the chosen particles. The increase in dN/dy for protons is very well seen in the data (see, e.g., Refs. [55–58]) and is reproduced by the

in different space-time domains [37–40]. These analyses were done for the whole time evolution rather than for the freeze-out as in this work.

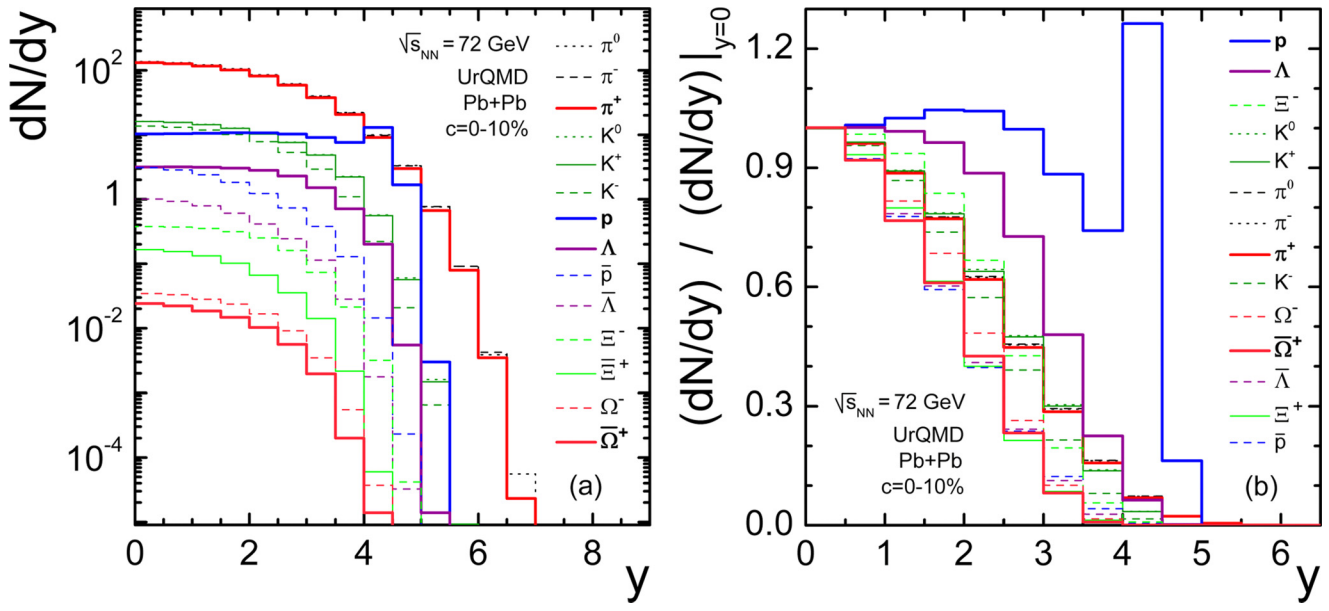

FIG. 1. (a) Rapidity dependence of particle multiplicities per event generated in the UrQMD model. The particle labels are sorted according to their abundance at $y = 0$. (b) The same as (a), but normalized to the corresponding value at midrapidity. The particle labels are sorted according to their abundance in the rapidity interval $2 < y < 2.5$.

UrQMD (see, e.g., Refs. [59,60]). The particle set is chosen in order to be able to constrain the HRG parameters in a thermal fit.

In our fits we use the THERMAL-FIST [61] thermal model package, previously used in Refs. [62,63]. A general description of an HRG model can be found following Refs. [64–66]. For recent applications of an HRG see, e.g., [67–69], and references therein. We consider only the grand canonical ensemble, thus, we imply that the baryon number B, electric charge Q, and strangeness of the system S are conserved on average. We assume no additional interactions between particles in an HRG, therefore excluded-volume [70–72] and van der Waals interaction effects [73] are omitted. This provides internal consistency of the procedure since these interactions are presently omitted in UrQMD as well. We expect strangeness nonequilibrium in small dN/dy bins, therefore, we do include the γ_S parameter [74] in fits. Thus, we have six parameters in the HRG: the system temperature T, the three chemical potentials μ_B, μ_Q, and μ_S, the γ_s, and the radius of the system R. The radius R is related to the system volume as $V = (4/3)\pi R^3$. Two chemical potentials, μ_Q and μ_S, are constrained for each considered rapidity bin by the conditions of zero net strangeness $\langle S \rangle = 0$ and by the ratio of electric charge to baryon charge of $\langle Q \rangle / \langle B \rangle \simeq 0.4$, as in Pb nuclei. Thus, the number of free parameters is four: T, μ_B, γ_s, and R. The set of the input mean multiplicities should contain all three conserved charges, mesons, baryons, and their antiparticles. Therefore we choose the following particle set, which satisfies these conditions: π^0, $\pi^\pm$, K^0, $K^\pm$, p, $\bar{p}$, Λ, $\bar{\Lambda}$, Ξ^-, $\bar{\Xi}^+$, Ω^-, $\bar{\Omega}^+$. A thermal fit requires both mean hadron yields and their uncertainties. The statistical uncertainty scales with the number of events as $1/\sqrt{N_{\rm ev}}$ and becomes very small for a large number of generated events. Therefore, we additionally assume theoretical *systematic* uncertainty at the level of 10% for each UrQMD-generated yield. This assumption for uncertainties is comparable to the total experimental uncertainties reported in the RHIC BES [75] and in ALICE [76,77].

Figure 2(a) shows the T and μ_B values obtained in a rapidity scan with the step $\Delta y = 0.5$ at a fixed energy ($\sqrt{s_{NN}} = 72$ GeV; open circles), in comparison with an energy scan at a fixed rapidity ($0 < y < 0.5$; open triangles). The energy scan corresponds to the RHIC BES program [75]. Note that we use the same mid-forward-rapidity interval $0 < y < 0.5$ in order to compare the energy scan and the rapidity scan in the UrQMD, while the RHIC BES results correspond to a symmetric and narrower interval, $-0.1 < y < 0.1$. In order to point out this difference we call our UrQMD beam energy scan "BES." The dN/dy yields used in the rapidity scan are shown in Fig. 1. The particle set for the fit of "BES" was limited to π^0, $\pi^\pm$, K^0, $K^\pm$, p, $\bar{p}$, Λ, $\bar{\Lambda}$, i.e., excluding the heavy Ξ^-, $\bar{\Xi}^+$ and Ω^-, $\bar{\Omega}^+$ (see the discussion of Fig. 3, below). The T and μ_B values obtained in the fit to the corresponding rapidity-integrated (4π) yields at $\sqrt{s_{NN}} = 72$ GeV are shown by the filled circle in Fig. 2(a). One can see that the integrated yields are similar to the average T and μ_B obtained in the rapidity scan in the moderate rapidity interval $0 < y < 3$. This is expected since the bulk of hadron production peaks at $y = 0$. The rapidity scan over all rapidities covers almost the same T and μ_B range as the energy scan at midrapidity.

Figure 2(b) depicts μ_B as a function of the rapidity. Triangles correspond to the whole particle set shown in Fig. 1; circles, to the set without Ξ and Ω as in Fig. 2(a). The results for μ_B appear to be almost independent of the particle set. This happens because the UrQMD was constrained to the rapidity distributions at various energies [59]. The increase in μ_B with y is caused by the data-driven increase in the baryon number dN/dy and by the decrease in dN/dy for other

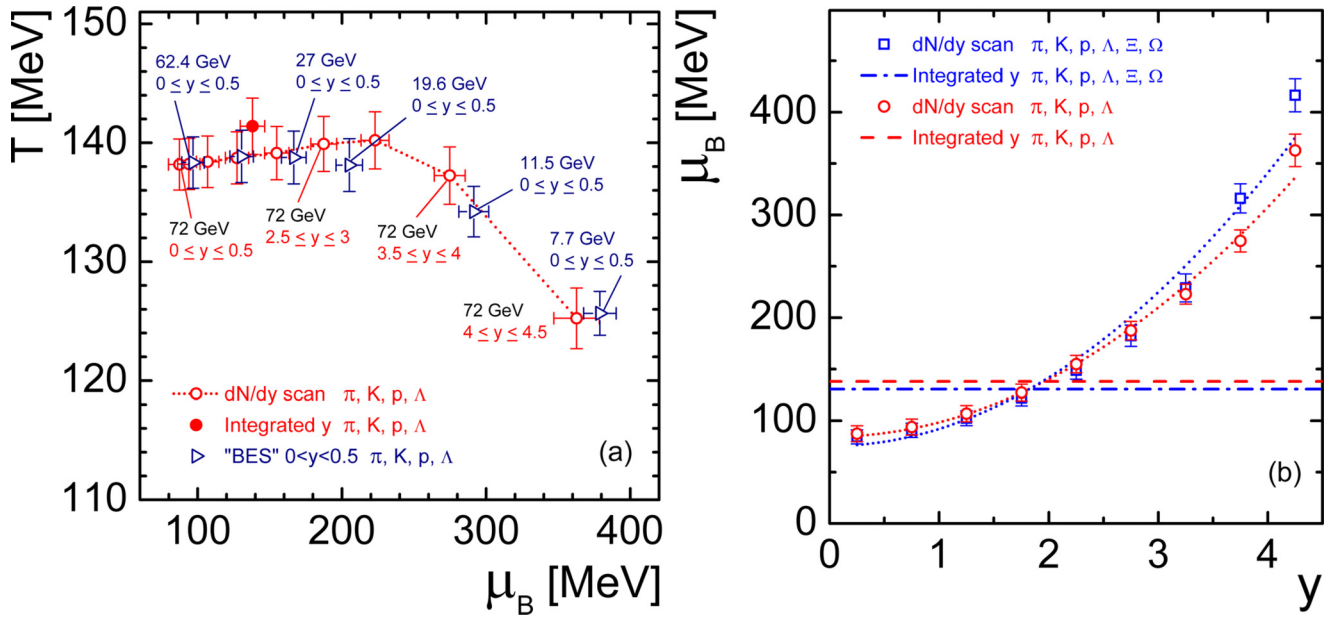

FIG. 2. (a) Rapidity scan at a fixed energy vs energy scan at a fixed rapidity. (b) μ_B as a function of rapidity.

particles at large y (see Fig. 1 and Refs. [55–58,78]). A similar increase in $\mu_B(y)$ was observed earlier at the top RHIC energy of $\sqrt{s_{NN}} = 200$ GeV and was fitted with a parabola [30,31],

$$\mu_B(y) = a + b\,y^2, \tag{1}$$

where the fit parameters were found to be $a = 25 \div 26$ MeV and $b = 11 \div 12$ MeV. We perform a similar parabolic fit to the extracted y dependence of μ_B at the AFTER@LHC energy [see dotted lines in Fig. 2(b)]. We obtain $a = 75.5 \pm 5.9$, $b = 16.6 \pm 1.0$ for the full particle set and $a = 84.5 \pm 3.2$, $b = 13.9 \pm 0.5$ for the set without Ξ and Ω. The a parameter is larger than in [30,31], because we study a lower collision energy (see [62,67,79,80]). The b parameter is similar to those in [30,31], with an indication of a stronger increase in μ_B at large y.

The chemical freeze-out temperature, $T(y)$, is approximately constant for the largest part of the rapidity interval considered, $y \lesssim 3$. Notable temperature changes appear only at larger rapidities, $y \gtrsim 3$, as shown in Fig. 3(a). If the Ξ and Ω UrQMD yields are considered in the thermal fit, then a pronounced peak in the $T(y)$ dependence is observed at $y \simeq 3.5$. This is required to describe these UrQMD yields with the HRG model. Analysis of the rapidity bin dependence shows that the peak in $T(y)$ is seen if the rapidity step is small

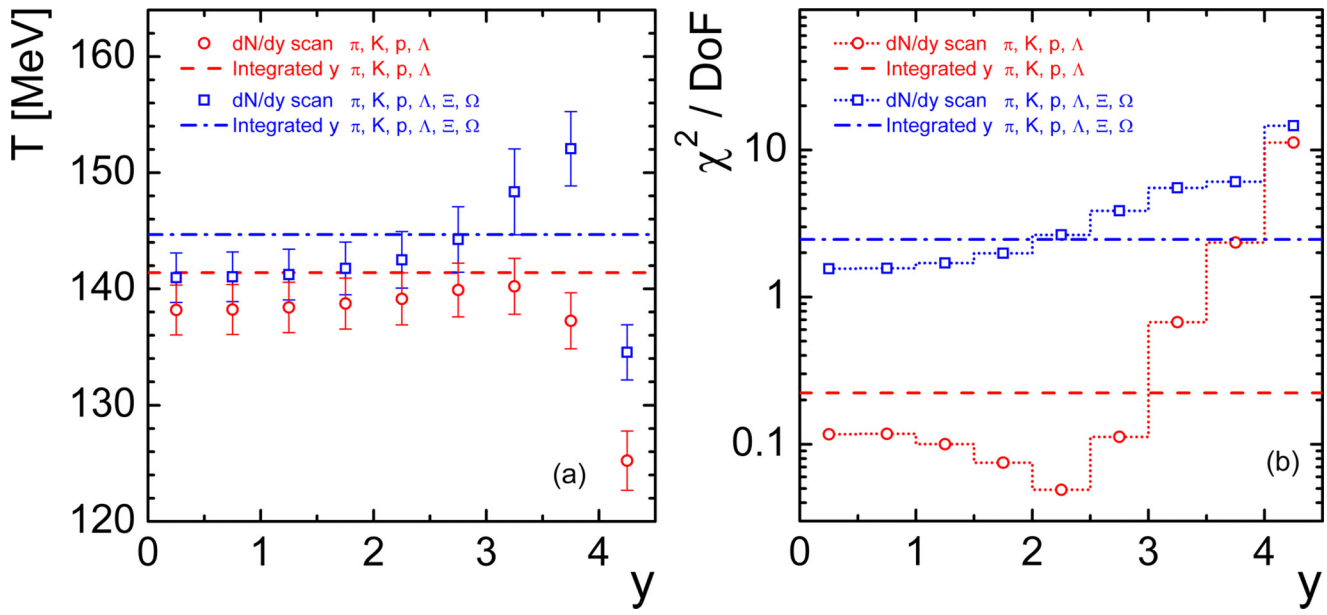

FIG. 3. (a) Extracted chemical freeze-out temperature and (b) χ^2 per degree of freedom as a function of the rapidity.

enough: $\Delta y \lesssim 2$. If Δy is decreased further, below the $\Delta y = 0.5$ currently employed, then the peak for $T(y)$ in Fig. 3(a) becomes slightly sharper. When the relative amount of Ξ, Ω, and other particles produced by UrQMD as a function of the rapidity can be confirmed or rejected experimentally, then it will ultimately be possible to say whether the maximum in $T(y)$ is an artifact of the modeling or a real effect. Note that the notable temperature changes shown in Fig. 3(a) correlate with a fast increase in χ^2/dof at $y \gtrsim 3$ [Fig. 3(b)], indicating that the interpretation of the corresponding large-rapidity bins in terms of temperature and baryochemical potential may be questionable. We note that in prior works it was assumed that $T(y) \simeq$ const [28,29], while the drop in T has also been reported in [30,31]. In contrast to our work, the increase in $T(y)$ with the rapidity is not observed in [30,31]. The reason is that the authors of [30,31] have enforced a parabolic increase in $\mu_B(y)$ and, also, enforced that T is a unique function of μ_B, such that the T-μ_B values always lie on the chemical freeze-out curve. This means that in [30,31] T always monotonically decreases by construction, as long as μ_B increases. We do not employ such a constraint in the present work.

The obtained temperature values are about 20 MeV smaller than the temperatures extracted from fits to the real data at the RHIC and LHC. In that regard one should note that the UrQMD contains string excitation and fragmentation, as well as many-body decays, which result in a Hagedorn-like equation of state in box simulations [81,82]. The temperature values that we observe, $T \sim 140$ MeV, appear to be caused by this property of the UrQMD model. Correcting for this UrQMD behavior, one arrives at $T \sim 150-160$ MeV as an estimate of the chemical freeze-out temperatures, as expected for the AFTER@LHC project from the common $T(\mu_B)$ freeze-out line [62,67,79,80].

The uncertainties of the HRG parameters result from the assumed 10% *systematic* uncertainties of the input multiplicities from the UrQMD. The freedom in choosing the input uncertainties means that the absolute values of χ^2 per degree of freedom depend on this assumption. However, the rapidity dependence of χ^2/dof tell us how good the treatment of the neighboring Δy bins as single fireballs is [see Fig. 3(b) and the discussion in the Appendix]. We do note that χ^2 values are smaller at small rapidities and show a rapid increase at large ($y > 2.5$) rapidities.

The largest relative increase in $\mu_B(y)$ obtained here for the AFTER@LHC project is a factor of about 5. This increase is reached between the smallest, $0 \lesssim y \lesssim 0.5$, and the largest, $4.0 \lesssim y \lesssim 4.5$, considered rapidity bins and for the particle set with Ξ and Ω, where this effect is the strongest [see squares in Fig. 2(b)]. However, the $\chi^2(y)$ of the thermal fit grows rapidly at $y \gtrsim 3$ [Fig. 3(b)], thus, the interpretation of these large-rapidity bins in terms of the HRG model may be doubtful. Therefore, let us denote the rapidity range $0 < y < 3$ the "conservative" one and the full considered rapidity range, $0 < y < 4.5$, the "optimistic" one. The temperature in the conservative rapidity range is the same for both particle sets, while the μ_B changes by *at least* a factor of 2.5. The change in μ_B in the "optimistic" range is much higher.

We checked that the change in μ_B with the rapidity can be expected to be even stronger in peripheral collisions, but also with a stronger dependence on the particle set used. The qualitative conclusion from the study of peripheral collision is similar. Therefore, we limit our study to the case of the most central collisions, for clarity.

The rapidity dependence of μ_B obtained here is determined by the dN/dy spectra produced by UrQMD. We use the UrQMD model in the cascade mode, without the intermediate hydro stage. Therefore, the main physics which determines the dN/dy spectra is embedded in the string excitation and fragmentation mechanism implementation in UrQMD and in the further transport of the baryon number and strangeness. There are many parameters which determine these mechanisms in UrQMD. They were fixed by the UrQMD Collaboration by fitting the various existing data at higher and at lower energies in elementary (hadron-hadron) and heavy-ion collisions. We do not vary these parameters and use the default ones. It is possible that the precise value of the relative increase in the baryon chemical potential can differ, if the UrQMD parameters are varied. The variation of these parameters would require additional assumptions and could break the existing agreement of the UrQMD model with the data, therefore it is not considered here.

The radius R and the strangeness saturation parameter γ_S behave as expected: they decrease with y (see Fig. 4). The values of R and γ_S are between the values obtained for the rapidity-integrated (4π) multiplicities measured in central Pb + Pb and in p + p collisions at the Super Proton Synchrotron energies [62,63]. The midrapidity values of R and γ_S resemble the Pb + Pb collisions, while the forward rapidities resemble p + p. This is due to the fact that the largest number of particles is produced at midrapidity, and their dN/dy values drop rapidly with increasing y (see Fig. 1). However, the radius parameter (i.e., the system volume) for the most forward considered rapidity bin is still much larger than that in p + p collisions (see [62,63]).

The rapidity-integrated (4π) multiplicities give the system radius for the full hadron set (with Ξ and Ω) as $R = 9.73 \pm 0.46$ fm, while for the set without Ξ and Ω the radius is $R = 10.54 \pm 0.48$ fm. This corresponds to system volumes of $V = 3864 \pm 543$ fm^3 (with Ξ and Ω) and $V = 4898 \pm 672$ fm^3 (no Ξ or Ω). The sum of the volumes obtained from the fits for the rapidity sub-bins is $V = 4225 \pm 210$ fm^3 (full hadron set) and $V = 5441 \pm 276$ fm^3 (no Ξ and Ω). Thus, the volume obtained for the fit of the rapidity-integrated yields agrees with the volume obtained after the sum of the sub-bin volumes. This indicates that the performed Δy binning is correct.

The comparison of the rapidity and the energy scan within the UrQMD shows that the rapidity scan within the interval $0 < y < 3$ will deliver systems which have temperatures, baryochemical potentials, volumes, and strangeness contents similar to those of systems obtained at midrapidity. The further increase in rapidity to $3 < y < 4.5$ will deliver systems which are at a similar temperature, with a larger baryon content, but with far fewer strange particles and in a smaller volume. The rapid increase in χ^2/dof at rapidities $y \gtrsim 3.5$ suggests that the corresponding y bins have less grounds to be treated in terms of the temperature and baryochemical potential compared to the rapidity bins at $y \lesssim 3.5$.

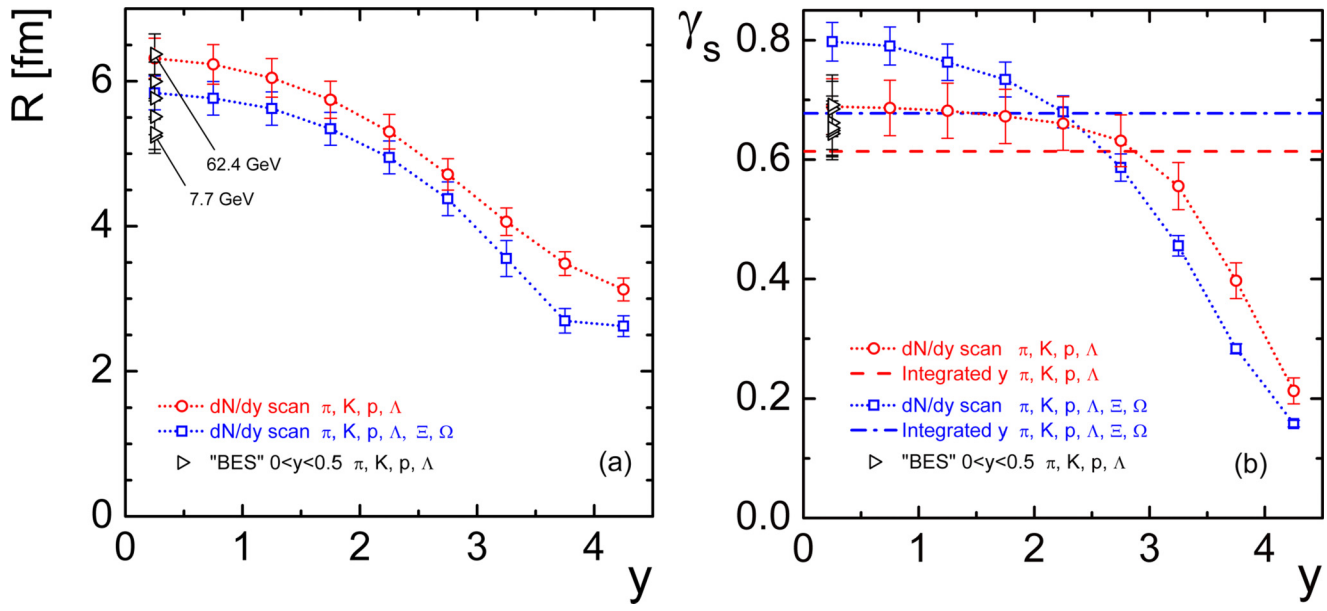

FIG. 4. (a) System radius parameter R and (b) strangeness saturation parameter γ_S as a function of the rapidity.

III. SUMMARY

We conclude that the dN/dy scan with Pb + Pb collisions at $\sqrt{s_{NN}} = 72\,\text{GeV}$ can be used to study systems which have similar temperatures, but at least a factor 2.5 larger baryon chemical potential in forward rapidity compared to midrapidity. The rapidity scan at the AFTER@LHC covers the majority of the μ_B range accessible in the RHIC Beam Energy Scan program.[2] Therefore, such a dN/dy study in the AFTER@LHC project will provide a complementary approach to the QCD phase diagram studies, with all the benefits of a high-luminosity fixed-target experiment at the LHC.

The integrated luminosity for Pb + Pb collisions at AFTER@LHC is $L_{\text{int}} \sim 1.6\,\text{nb}^{-1}$ [49] per year, which corresponds to ≈ 11.5 billion minimum bias events. Given the particle yields predicted by the UrQMD, and assuming even a very conservative value of the reconstruction efficiency of 1% [76,84] in the ALICE detector, the measurement precision of all particle species (except for the heaviest and the infrequent $\bar{\Omega}$) yields over the whole rapidity range considered here will be limited only by the systematic uncertainties. Only study of the $\bar{\Omega}$ baryon at the most forward rapidity bin could be a challenge, since the yield from the UrQMD model is low, and the success will depend on the $\Omega(\bar{\Omega})$ reconstruction efficiency available in the fixed-target mode. With a 4% reconstruction efficiency, and assuming a signal-to-background ratio of 3:1 [76] and the yield per event predicted by the UrQMD model, it will be possible to measure $\bar{\Omega}$ with 10% relative uncertainty. Thus, the studies proposed here are definitely within the reach of a single-year Pb + Pb program at the AFTER@LHC.

[2]In the late stages of preparation of this paper an article [83] appeared on arXiv. That paper covers a similar topic and reaches similar conclusions, but with a different method. Relativistic hydrodynamics is employed in [83] instead of transport simulation. In contrast to [83], here we additionally report on the degree of strangeness nonequilibrium and on the size of the system at freeze-out.

ACKNOWLEDGMENTS

The authors thank M. Gazdzicki, M. I. Gorenstein, K. Grebieszkow, and J. Steinheimer for fruitful discussions. D.K. gratefully acknowledges inspiring discussions with Jean-Philippe Lansberg.

APPPENDIX

Let us consider a single thermal source at rest [85]. The invariant momentum spectrum of particles radiated by this source is

$$E\frac{d^3N}{d^3p} = \frac{dN}{dy\,m_T\,dm_T\,d\phi} = \frac{gV}{(2\pi)^3}\,E\,e^{-(E-\mu)/T}, \quad \text{(A1)}$$

where $E = \sqrt{m^2+p^2} = m_T\cosh(y)$ is the energy of a particle with mass m and momentum p; y and ϕ are the rapidity and azimuthal angle of the particle's 4-momentum; $m_T = \sqrt{m^2+p_T^2}$ and p_T are, respectively, the transverse mass and transverse momentum; g and μ, the degeneracy factor of a particle and the chemical potential; and V and T, the volume and temperature of the system. The integration over ϕ and m_T in Eq. (A1) yields the rapidity distribution

$$\begin{aligned}\frac{dN}{dy} &= \int \frac{gV}{(2\pi)^3}\,E\,e^{-(E-\mu)/T} m_T\,dm_T\,d\phi \\ &= \frac{V}{(2\pi)^2}\cosh(y)\,e^{\mu/T}\int_m^\infty e^{-m_T\cosh(y)/T} m_T^2\,dm_T \\ &= \frac{gV}{(2\pi)^2}\,T^3\,e^{\mu/T}\left(\frac{2}{[\cosh(y)]^2} + \frac{m}{T}\,\frac{2}{\cosh(y)} \right. \\ &\quad \left. + \frac{m^2}{T^2}\right)e^{-\frac{m}{T}\cosh(y)}. \end{aligned} \quad \text{(A2)}$$

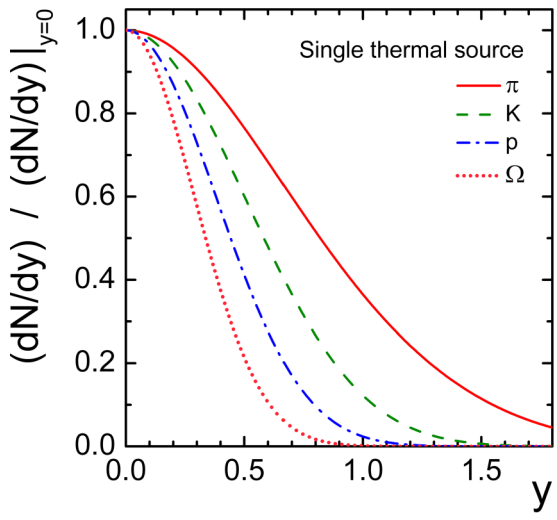

FIG. 5. Normalized rapidity distribution produced by a single thermal source at $T = 140$ MeV.

Equation (A2) contains the dependence on the particle's mass. We plot it in Fig. 5 for $T = 140$ MeV, $\mu = 0$, and $m =$ 140, 494, 938, and 1672 MeV, which correspond, respectively, to pions, kaons, protons, and Ω baryons. One may see that a single thermal source produces very different rapidity distributions for particles with different masses. The larger the mass, the narrower is the distribution. Therefore, the selection of a narrow rapidity bin and a fit of the particle multiplicities from this bin would produce a temperature and other parameters which are different from those of the whole fireball. A midrapidity cut would increase the number of heavy particles relative to light ones, while a forward rapidity cut would decrease it. This behavior is qualitatively similar to the decrease in γ_S with the rapidity in our analysis of the UrQMD-generated output, because strange particles are heavier than nonstrange.

However, the dN/dy distributions that are produced in experiments (and also in the UrQMD model) are not from a single thermal source (compare Fig. 1 and Fig. 5). The rapidity distributions from a static thermal source have a Gaussian-like shape, with the full width at half-maximum $\Delta y_{\rm FB} \simeq 1.6$, 1.2, 0.9, and 0.7 for pion, kaon, proton, and Ω, respectively. In contrast, the UrQMD-generated dN/dy distributions have a wide plateau at midrapidity, $dN/dy \sim$ const in the interval $\Delta y \gg \Delta y_{\rm FB}$. This is the manifestation of a boost invariance of multiplicity distributions at midrapidity in high-energy reactions. It also means that the wide dN/dy distributions produced by an experiment or by the UrQMD can be approximated with a sum of thermal fireballs populating the rapidity axis, as done for $\sqrt{s_{NN}} = 200$ GeV at the RHIC in [28–31].

Typically, the HRG model has been applied in two extreme cases as far as the rapidity scan is concerned: in the full rapidity interval and for a very narrow midrapidity. We propose to treat each sub-bin as a separate fireball and decide about the quality of this approximation by looking at the χ^2/dof values. Application of this procedure is much simpler than the fits of the dN/dy with the sum of the fireballs. The change in the output HRG parameters in our case will indicate which particles are present at which rapidity and to what extent the selected rapidity bin can be treated as a single fireball.

[1] S. V. Afanasiev *et al.* (NA49 Collaboration), Phys. Rev. C **66**, 054902 (2002).
[2] K. Adcox *et al.* (PHENIX Collaboration), Nucl. Phys. A **757**, 184 (2005).
[3] B. B. Back *et al.*, Nucl. Phys. A **757**, 28 (2005).
[4] I. Arsene *et al.* (BRAHMS Collaboration), Nucl. Phys. A **757**, 1 (2005).
[5] J. Adams *et al.* (STAR Collaboration), Nucl. Phys. A **757**, 102 (2005).
[6] B. B. Abelev *et al.* (ALICE Collaboration), J. High Energy Phys. 06 (2015) 190.
[7] G. Aad *et al.* (ATLAS Collaboration), Phys. Lett. B **707**, 330 (2012).
[8] K. Aamodt *et al.* (ALICE Collaboration), Phys. Lett. B **696**, 30 (2011).
[9] G. Aad *et al.* (ATLAS Collaboration), Phys. Rev. Lett. **105**, 252303 (2010).
[10] S. Chatrchyan *et al.* (CMS Collaboration), Phys. Rev. C **84**, 024906 (2011).
[11] Y. Aoki, G. Endrodi, Z. Fodor, S. D. Katz, and K. K. Szabo, Nature **443**, 675 (2006).
[12] S. Borsanyi *et al.*, J. High Energy Phys. 11 (2010) 077.
[13] A. Bazavov, T. Bhattacharya, M. Cheng, C. De Tar, H.-T. Ding, S. Gottlieb, R. Gupta, P. Hegde, U. M. Heller, F. Karsch, E. Laermann, L. Levkova, S. Mukherjee, P. Petreczky, C. Schmidt, R. A. Soltz, W. Soeldner, R. Sugar, D. Toussaint, W. Unger, and P. Vranas (HotQCD Collaboration), Phys. Rev. D **85**, 054503 (2012).
[14] S. P. Klevansky, Rev. Mod. Phys. **64**, 649 (1992).
[15] A. Barducci, R. Casalbuoni, G. Pettini, and R. Gatto, Phys. Rev. D **49**, 426 (1994).
[16] M. A. Stephanov, Phys. Rev. Lett. **76**, 4472 (1996).
[17] M. G. Alford, K. Rajagopal, and F. Wilczek, Phys. Lett. B **422**, 247 (1998).
[18] M. A. Stephanov, K. Rajagopal, and E. V. Shuryak, Phys. Rev. Lett. **81**, 4816 (1998).
[19] M. A. Stephanov, Prog. Theor. Phys. Suppl. **153**, 139 (2004); Int. J. Mod. Phys. A **20**, 4387 (2005).
[20] D. Keane, J. Phys. Conf. Ser. **878**, 012015 (2017).
[21] The STAR Collaboration, https://drupal.star.bnl.gov/STAR/starnotes/public/sn0598.
[22] L. Turko (for the NA61/SHINE Collaboration), Universe **4**, 52 (2018).
[23] V. Golovatyuk, V. Kekelidze, V. Kolesnikov, O. Rogachevsky, and A. Sorin, Eur. Phys. J. A **52**, 212 (2016).
[24] T. Ablyazimov *et al.* (CBM Collaboration), Eur. Phys. J. A **53**, 60 (2017).
[25] H. Sako (J-PARC Heavy-Ion Collaboration), JPS Conf. Proc. **8**, 022010 (2015).
[26] N. G. Antoniou, F. K. Diakonos, X. N. Maintas, and C. E. Tsagkarakis, Phys. Rev. D **97**, 034015 (2018).

[27] A. Dumitru, D. H. Rischke, T. Schonfeld, L. Winckelmann, H. Stocker, and W. Greiner, Phys. Rev. Lett. **70**, 2860 (1993).
[28] B. Biedron and W. Broniowski, Phys. Rev. C **75**, 054905 (2007).
[29] W. Broniowski and B. Biedron, J. Phys. **G35**, 044018 (2008).
[30] F. Becattini, J. Cleymans, and J. Strumpfer, PoS **CPOD07**, 012 (2007).
[31] F. Becattini and J. Cleymans, J. Phys. **G34**, S959 (2007).
[32] M. Li and J. I. Kapusta, Phys. Rev. C **95**, 011901 (2017).
[33] Y. B. Ivanov and A. A. Soldatov, Phys. Rev. C **98**, 014906 (2018).
[34] J. Brewer, S. Mukherjee, K. Rajagopal, and Y. Yin, arXiv:1804.10215.
[35] The AFTER@LHC Study Group, http://after.in2p3.fr.
[36] D. Kikola, Quark Matter, in press (2018).
[37] L. V. Bravina *et al.*, Phys. Lett. B **434**, 379 (1998).
[38] L. V. Bravina *et al.*, J. Phys. **G25**, 351 (1999).
[39] L. V. Bravina, E. E. Zabrodin, M. I. Gorenstein, S. A. Bass, M. Belkacem, M. Bleicher, M. Brandstetter, C. Ernst, M. Hofmann, L. Neise, S. Soff, H. Weber, H. Stöcker, and W. Greiner, Phys. Rev. C **60**, 024904 (1999).
[40] S. Endres, H. van Hees, J. Weil, and M. Bleicher, Phys. Rev. C **91**, 054911 (2015).
[41] S. A. Bass *et al.*, Prog. Part. Nucl. Phys. **41**, 255 (1998); **41**, 225 (1998).
[42] M. Bleicher *et al.*, J. Phys. **G25**, 1859 (1999).
[43] K. C. Meehan (STAR Collaboration), Nucl. Phys. A **956**, 878 (2016).
[44] K. Meehan (STAR Collaboration), Nucl. Phys. A **967**, 808 (2017).
[45] R. Aaij *et al.* (LHCb Collaboration), Eur. Phys. J. C **72**, 2168 (2012).
[46] R. Aaij *et al.* (LHCb Collaboration), J. High Energy Phys. 08 (2011) 034.
[47] E. Maurice (LHCb Collaboration), in *5th Large Hadron Collider Physics Conference (LHCP 2017), Shanghai, China, May 15–20, 2017*, in press (2018).
[48] G. Graziani (LHCb Collaboration), in *52nd Rencontres de Moriond on Electroweak Interactions and Unified Theories, La Thuile, Italy, 18–25 March 2017*, Report number LHCb-CONF-2017-002 (2017).
[49] L. Massacrier *et al.*, EPJ Web Conf. **171**, 10001 (2018).
[50] L. Massacrier *et al.*, Adv. High Energy Phys. **2015**, 986348 (2015).
[51] S. J. Brodsky, F. Fleuret, C. Hadjidakis, and J. P. Lansberg, Phys. Rep. **522**, 239 (2013).
[52] D. Kikola *et al.*, Few Body Syst. **58**, 139 (2017).
[53] B. Trzeciak *et al.*, Few Body Syst. **58**, 148 (2017).
[54] D. Kikola, Adv. High Energy Phys. **2015**, 783134 (2015).
[55] H. Appelshauser *et al.* (NA49 Collaboration), Phys. Rev. Lett. **82**, 2471 (1999).
[56] I. C. Arsene *et al.* (BRAHMS Collaboration), Phys. Lett. B **677**, 267 (2009).
[57] F. Videbaek (BRAHMS Collaboration), Nucl. Phys. A **830**, 43c (2009).
[58] T. Anticic *et al.* (NA49 Collaboration), Eur. Phys. J. C **65**, 9 (2010).
[59] M. Mitrovski, T. Schuster, G. Graf, H. Petersen, and M. Bleicher, Phys. Rev. C **79**, 044901 (2009).
[60] V. Ozvenchuk and A. Rybicki, Nucl. Phys. A **973**, 104 (2018).
[61] The THERMAL-FIST package, https://github.com/vlvovch/Thermal-FIST.
[62] V. Vovchenko, V. V. Begun, and M. I. Gorenstein, Phys. Rev. C **93**, 064906 (2016).
[63] V. V. Begun, V. Vovchenko, M. I. Gorenstein, and H. Stoecker, arXiv:1805.01901.
[64] S. Wheaton and J. Cleymans, Comput. Phys. Commun. **180**, 84 (2009).
[65] G. Torrieri *et al.*, Comput. Phys. Commun. **167**, 229 (2005).
[66] M. Petran, J. Letessier, J. Rafelski, and G. Torrieri, Comput. Phys. Commun. **185**, 2056 (2014).
[67] A. Andronic, P. Braun-Munzinger, K. Redlich, and J. Stachel, arXiv:1710.09425.
[68] M. Bleicher, J. Steinheimer, and R. Stock, *The QCD Phase Diagram from Statistical Model Analysis* (World Scientific Publishing Co. Pte. Ltd., Singapore, 2018), pp. 41–64.
[69] S. Chatterjee, A. K. Dash, and B. Mohanty, J. Phys. **G44**, 105106 (2017).
[70] D. H. Rischke, M. I. Gorenstein, H. Stoecker, and W. Greiner, Z. Phys. C **51**, 485 (1991).
[71] G. D. Yen, M. I. Gorenstein, W. Greiner, and S.-N. Yang, Phys. Rev. C **56**, 2210 (1997).
[72] G. D. Yen and M. I. Gorenstein, Phys. Rev. C **59**, 2788 (1999).
[73] V. Vovchenko, M. I. Gorenstein, and H. Stoecker, Phys. Rev. Lett. **118**, 182301 (2017).
[74] J. Letessier, A. Tounsi, U. W. Heinz, J. Sollfrank, and J. Rafelski, Phys. Rev. D **51**, 3408 (1995).
[75] L. Adamczyk *et al.* (STAR Collaboration), Phys. Rev. C **96**, 044904 (2017).
[76] B. B. Abelev *et al.* (ALICE Collaboration), Phys. Lett. B **728**, 216 (2014) [**734**, 409(E) (2014)].
[77] B. Abelev *et al.* (ALICE Collaboration), Phys. Rev. C **88**, 044910 (2013).
[78] T. Anticic *et al.* (NA49 Collaboration), Phys. Rev. C **94**, 044906 (2016).
[79] J. Cleymans and K. Redlich, Phys. Rev. Lett. **81**, 5284 (1998).
[80] A. Andronic, P. Braun-Munzinger, and J. Stachel, Nucl. Phys. A **772**, 167 (2006).
[81] M. Belkacem, M. Brandstetter, S. A. Bass, M. Bleicher, L. Bravina, M. I. Gorenstein, J. Konopka, L. Neise, C. Spieles, S. Soff, H. Weber, H. Stöcker, and W. Greiner, Phys. Rev. C **58**, 1727 (1998).
[82] E. Zabrodin, L. Bravina, M. Bleicher, and H. Stöcker, EPJ Web Conf. **126**, 03006 (2016).
[83] I. Karpenko, arXiv:1805.11998.
[84] K. Aamodt *et al.* (ALICE Collaboration), Eur. Phys. J. C **71**, 1594 (2011).
[85] E. Schnedermann, J. Sollfrank, and U. W. Heinz, Phys. Rev. C **48**, 2462 (1993).